Baroclinic Empirical Orthogonal Functions as Basis Functions in an Atmospheric Model

FRANK M. SELTEN

Royal Netherlands Meteorological Institute, De Bilt, the Netherlands

(Manuscript received 28 August 1995, in final form 17 September 1996)

ABSTRACT

In this study, empirical orthogonal functions (EOFs) are used as basis functions in a spectral model of the atmospheric circulation. Two hypotheses are tested. The first hypothesis is that a basis of EOFs is more efficient in describing large-scale atmospheric dynamics compared to spherical harmonics. The second hypothesis is that, by using EOFs as basis functions, the forecast skill and climatology of the model can be improved.

Two experiments are performed with a three-level, quasigeostrophic, hemispheric spectral T21 model. In the first experiment, a perfect model approach is taken. In the second, T21 is used to produce forecasts for the Northern Hemisphere in winter. In the perfect model experiment, EOFs are determined from a long model integration; in the second experiment, EOFs are determined from 10 winters of ECMWF analyses.

The first hypothesis is tested by comparing the forecast skill of EOF truncated versions of T21 with the skill of a T17 version. In both experiments it is found that with less than half the number of degrees of freedom the EOF model beats T17. However, although the EOF model is more efficient with respect to the number of degrees of freedom, it is more expensive to integrate numerically.

The second hypothesis is tested in the perfect model experiment by producing forecasts of the T21 circulation with T17, filtered on the leading EOFs, in an attempt to reduce the error propagation from the trailing EOFs and thus improve the forecast skill of T17. In contrast to previously obtained results in the barotropic case, the filter does not improve the forecast skill. With an empirically determined dissipation on the EOFs as a closure for neglected interactions, both the forecast skill and the climatology of T17 show some improvement. In the second experiment T21 is filtered on the leading atmospheric EOFs. Also in this experiment, the EOF filter does not improve the forecast skill of T21. By introducing an empirically determined dissipation on the EOFs, the variability of T21 shows some improvement.

1. Introduction

In order to predict a future state of the atmosphere, a model of the atmosphere is integrated forward in time, starting from an ''observed'' initial state. The predicted evolution diverges from the observed one due to the amplification of small errors in the initial state, often referred to as internal error growth, and due to imperfections of the model (see Boer 1984). These model errors not only contribute to the forecast error but also lead to climate drift: the attractor of the model differs from the atmospheric attractor. Climate drift shows up in, for example, too intense storms, too little blocking activity, no southern oscillation or sudden stratospheric warmings, errors in the mean position, amplitude of the stationary planetary waves, and so on. One way to diagnose climate drift is to calculate empirical orthogonal functions (EOFs). EOFs efficiently describe the attractor [see Selten (1995b) for a discussion of EOFs of the Lorenz (1963) attractor]. Changes in the attractor are reflected in changes in the amount of variance associated with each EOF. One way to reduce climate drift would be to adjust the model equations in order to obtain the right amount of variance for each EOF. In Selten (1995a) two promising results were obtained with respect to the effect of the model error on forecast skill and on the ability to simulate the climate. In the following we will refer to this paper as SE. In SE, a T21 barotropic model was regarded as truth. EOFs were calculated from a 50 000-day integration. Model errors were introduced by truncating the model to T20. The T20 version was used to forecast the T21 circulation. The model error of T20 caused a systematic increase of the variance of the trailing EOFs during the first couple of days of the forecasts. Putting the amplitude of the trailing EOFs to zero after each day of integration substantially improved the forecast skill of the leading EOFs. Apparently, this EOF filter slowed down the error propagation from the trailing EOFs to the leading ones. In a second experiment in the same paper, evolution equations were derived for the leading 20 (out of 231) EOFs. Integrating this reduced model, starting from many different initial conditions on the attractor of T21, it was found that the variance of almost all EOFs systematically increased

Corresponding author address: Frank M. Selten, Royal Netherlands Meteorological Institute, P.O. Box 201, 3730 AE De Bilt, the Netherlands.
E-mail: selten@knmi.nl

during the integration. The mean state and the variability pattern, determined from a 10-y integration with the low-order EOF model, differed substantially from T21. By adjusting the linear dissipation on each EOF such as to balance the mean initial drift of the associated variance, the reduced model reproduced the mean and variability quite well.

EOFs have been shown to efficiently describe barotropic dynamics (Rinne and Karhilla 1975; Schubert 1985; SE), but it remains to be seen whether EOFs are suitable basis functions in more realistic models of the atmospheric circulation. In this study, we investigate the merits of using EOFs as basis functions in a quasigeostrophic, baroclinic three-level model, truncated to T21. More specifically, two hypotheses are tested. First, it is hypothesized that a basis of EOFs is more efficient in describing the dynamics compared to spherical harmonics. Second, it is hypothesized that by using EOFs as basis functions, the effect of model errors can be reduced, leading to an improved forecast skill and climatology of the model. Due to model errors, model attractors differ from the atmospheric attractor. This difference shows up in the variance associated with each of the EOFs. In general, the trailing EOFs gain variance. It is hypothesized that either removing the trailing EOFs or increasing the dissipation on the EOFs improves the forecast skill and climatology of the atmospheric model, since the model trajectory is confined to that part of phase space where the atmospheric attractor resides.

Each hypothesis is tested in two experiments. In the first experiment, a perfect model approach is taken; the T21 model is regarded as perfect and model errors are introduced by truncating the model to T17. In the second experiment, T21 is used to simulate the Northern Hemisphere winter circulation. In the perfect model experiment, EOFs are determined from a long model integration, in the second experiment the EOFs are determined from 10 winters of ECMWF analyses. The motivation for doing these two experiments is that the model error is quite different in both experiments. In the perfect model experiment, the only model error is a reduced horizontal resolution. In the second experiment, other model error sources are involved like the coarse vertical resolution, the representation of diabatic sources and sinks by an empirically determined constant potential vorticity forcing, the parameterization of orographic effects, and the quasigeostrophic approximation.

This paper is organized as follows. Section 2 presents a brief description of the T21 model. In section 3 an explanation is given of how the EOFs are calculated, followed by a discussion of their properties, both for the EOFs of the model data and the ECMWF analyses. In section 4, the EOF filter is introduced and it is explained how the EOF dissipation is determined. The first hypothesis is tested in both experiments in section 5, in section 6 the second hypothesis. Conclusions and some discussion of the results are presented in section 7.

2. The model

The quasigeostrophic, baroclinic T21 model used in this study is the one described in Marshall and Molteni (1993). It consists of three equations describing the time evolution of quasigeostrophic potential vorticity Q at pressure levels 200 hPa, 500 hPa, and 800 hPa, respectively. For details on the model formulation we refer to Marshall and Molteni (1993). The model was made hemispheric by antisymmetrization of the orography field multiplied by the Coriolis parameter and the orography dependent diffusion at the lowest level with respect to the equator. The model contains a scale-selective horizontal ∇^8 diffusion on Q to prevent accumulation of energy near the truncation limit. This diffusion has an e-folding timescale of one day at the largest wavenumber 21. Without scale-selective diffusion, the variance of Q at the tail of the spectrum rapidly increases during a model integration starting from an analyzed initial condition. With the mentioned scale-selective diffusion, the model is able to simulate the observed spectrum of the variance of Q quite well for high wavenumbers. A constant vorticity forcing term is calculated from 10 winters of ECMWF analyses such that the mean vorticity tendency generated by the model is zero, as in Liu and Opsteegh (1994). The model is integrated forward in time using a fourth-order Runge Kutta scheme with a time step of four hours. With this empirical forcing, the model is able to simulate the Northern Hemisphere winter climatology and variability reasonably well.

3. Empirical orthogonal functions

a. Definition

EOFs are determined from a set of observations of the system under study. EOFs of the T21 model are estimated from a dataset produced as follows. Starting from a state of rest, the model was integrated for 1000 days. Assuming the model had reached its attractor, it was integrated for another 10 000 days. Once each day, the model state was archived. At T21 resolution, the state is completely specified by the 693 spherical harmonic coefficients of the streamfunction expansion (231 coefficients at each level). Put differently, the phase space of the model is 693-dimensional. EOFs of the atmosphere are estimated from 10 boreal winters of ECMWF analyses (DJF 1983/84 to 1992/93) of 200-, 500-, and 800-hPa streamfunctions in the Northern Hemisphere at T21 resolution.

The EOFs were defined as follows: We choose to calculate EOFs from the geopotential field in order to focus on the extratropical areas. Relating the geopotential height Φ to the streamfunction field Ψ by the linear balance equation, the geopotential height is formally given by

$$\Phi = L\Psi, \tag{1}$$

where L denotes a linear operator. On a hemispheric domain, the operator L is invertible. Since we want to calculate EOFs for the three levels simultaneously, in order to incorporate vertical correlations into the EOF structures we need to make a choice on how the three levels are weighted. In order to get, at a given truncation, the same relative representation error in the geopotential fields at the three levels, we choose the weights such that all three levels have the same amount of variance. So we solve the eigenvalue equation

$$L\overline{\Psi'\Psi'^{T}}L^{T}\,\mathbf{M}e_i = \lambda_i e_i \qquad (2)$$

for the EOFs e_i and the corresponding eigenvalues λ_i. The overbar denotes a time average and $\mathbf{M}$ denotes a diagonal matrix containing weights that depend on the dataset. The primes indicate that the time mean has been subtracted. The dimension of the covariance matrix is 693.

b. EOFs of the T21 model

The covariance matrix was estimated from the 10 000-day dataset and Eq. (2) was solved for the EOFs and the eigenvalues.

1) EIGENVALUES

A plot of the eigenvalues is given in Fig. 1a. The eigenvalue spectrum is steep: 70 EOFs acount for 95% of the variance. It implies that on average the model state is rather well described with a limited number of EOFs. To get an idea of the accuracy of the representation of the state vector with a limited number of EOFs, we calculated the rms error as a function of the number of EOFs (Fig. 1b). With 150 EOFs, the mean representation error at 200 hPa is about 15 m, at 500 hPa about 13 m, and at 800 hPa 9 m. This error was calculated from 200 days, separated by intervals of 10 days, taken from an independent dataset of 2500 days. Thus an arbitrary model state on the attractor is rather well described using 150 EOFs. It remains to be seen whether the dynamics on the attractor is also well described using 150 EOFs.

2) SPACE AND TIME CHARACTERISTICS

The EOFs are optimized with respect to the variance. Since the variance is dominated by low-frequency fluctuations of large-scale structures, the EOFs are a time and a spatial filter. To illustrate this, we calculated for each EOF amplitude the autocorrelation from the 10 000-day dataset. In Fig. 2a, the lag is plotted at which the autocorrelation drops below 0.8 and 0.6, respectively, for each of the EOFs. It is evident that the time evolution becomes faster with increasing EOF index. Note that at the tail of the spectrum the decorrelation time tends to increase again. Since this behavior is not found in case of atmospheric EOFs (see Fig. 5a) and

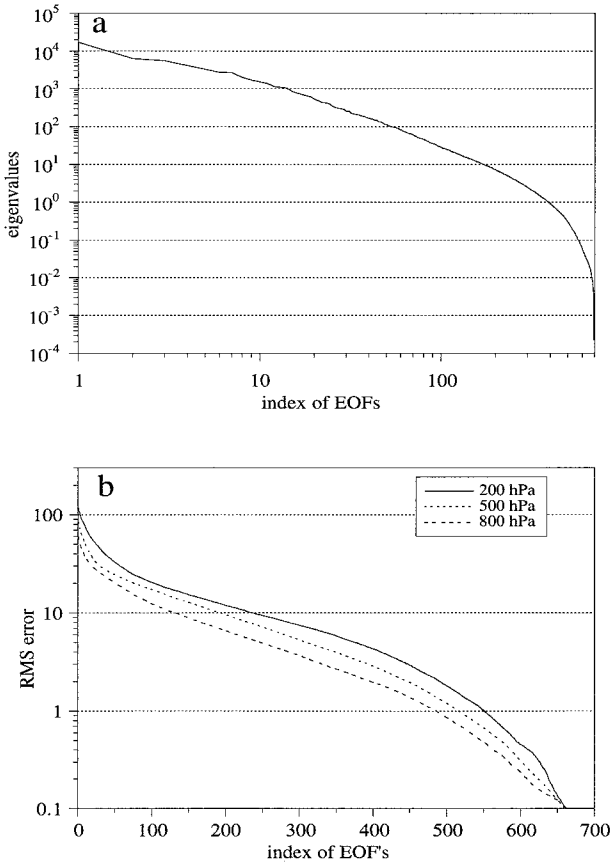

FIG. 1. (a) Eigenvalues (or variances) [m^2] of the EOFs determined from a 10 000-day time series of the T21 model. (b) Mean representation error [m] of 200-hPa, 500-hPa, and 800-hPa geopotential height due to EOF truncation.

since it happens at the end of the spectrum, it is probably caused by the inability of the model to correctly evolve the modes near the truncation limit.

To get an idea of the spatial scales, we calculated for each EOF a weighted mean wavenumber

$$\bar{n} = \frac{1}{21}\sum_{n=1}^{21}\frac{\phi_n^2}{\sum_{n'=1}^{21}\phi_{n'}^2}n, \qquad (3)$$

where ϕ_n denotes the total projection of the EOF onto spherical harmonics with total wavenumber n. The results are plotted in Fig. 2b as a function of the EOF index for the 500-hPa level. The graph shows that the dominant EOFs are dominated by large-scale structures, whereas trailing EOFs are dominated by smaller-scale structures.

Given the large difference in energy content and time and spatial scales, it is to be expected that the influence of the trailing EOFs on the leading ones is negligibly small, at least on short timescales. The extent to which this is true will be investigated in sections 5 and 6.

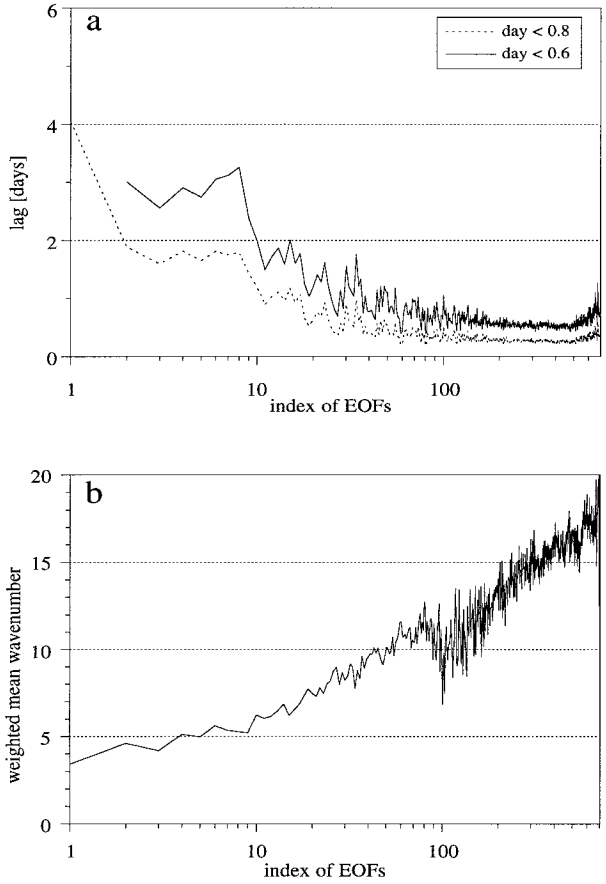

FIG. 2. (a) Lag in days at which the autocorrelation of the EOF amplitudes drops below 0.8 and 0.6, respectively. (b) Spatial-scale dependence of the EOFs as characterized by a weighted mean wavenumber.

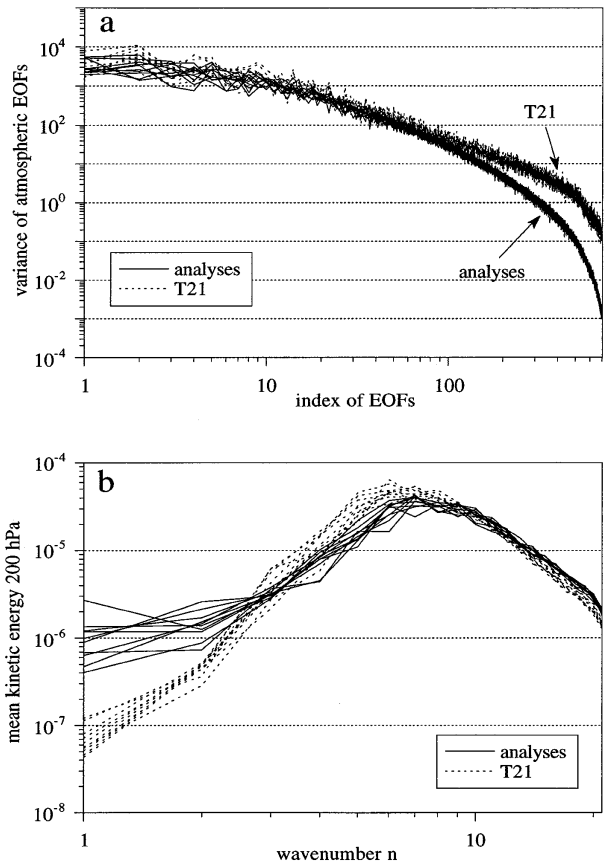

FIG. 3. Variances of EOFs from observations (DJF 1983–92 ECMWF analyses) for each of the 10 winters and the variances of these EOFs in 10 independent 90-day periods in the 10 000-day time series of T21. (b) Kinetic energy spectrum at 200 hPa for each of the 10 winters of ECMWF analyses for anomalies with respect to the winter mean and kinetic energy spectra for 10 independent 90-day periods in the 10 000-day time series of T21.

3) VERTICAL STRUCTURE

A final characteristic of the EOFs that we would like to discuss is their vertical structure. For each of the EOFs we calculated the pattern correlation between the different pressure levels. For the first several tens of EOFs, the correlation between the different levels is around 0.9. This indicates an equivalent barotropic structure. Then the correlations drop to smaller values and become slightly negative, indicating a more baroclinic structure. There are no large negative correlations between the levels for any of the EOFs. Apparently, the norm that we have chosen to define for these EOFs favors equivalent barotropic structures. If we had chosen the total energy norm, which puts more weight on the temperature structure, we would have found more pronounced baroclinicity in the leading EOFs. As discussed in Selten (1993), this has consequences for the energy cycle in a truncated EOF model. Both the velocity fields as well as temperature fields need to be well represented in order to describe the energy conversion correctly. To check how many EOFs are needed to accurately describe the temperature field, we calculated the mean represen-

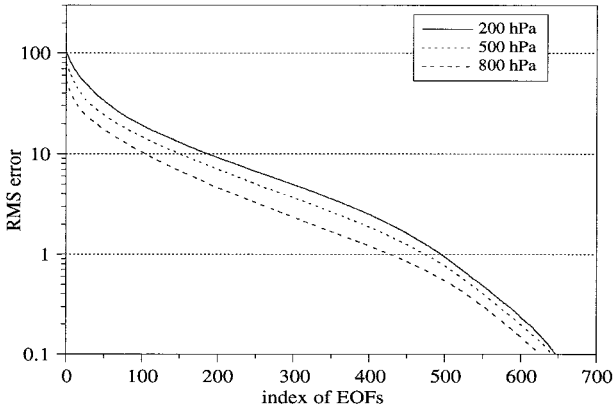

FIG. 4. Mean representation error of 200-, 500- and 800-hPa geopotential height of ECMWF winter analyses due to EOF truncation. Values below 0.1 m are not shown.

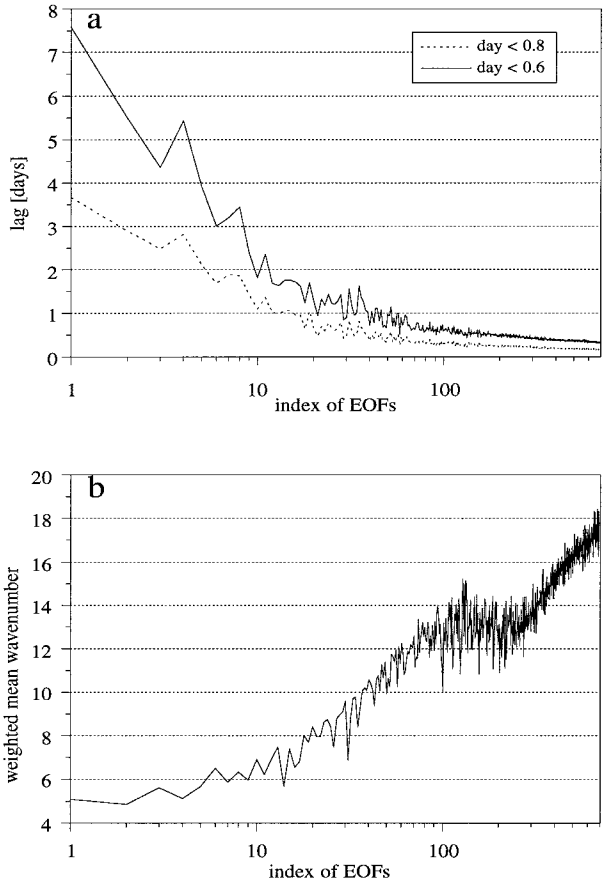

FIG. 5. (a) Lag in days at which the autocorrelation of the EOF amplitudes drop below 0.8 and 0.6, respectively. (b) Spatial-scale dependence of the EOFs as characterized by a weighted mean wavenumber.

tation error in the 200–500 hPa and 500–800 hPa thickness as a function of the number of EOFs in the expansion (not shown). It turned out that more EOFs (about 300) are needed to represent the temperature fields with similar accuracy as the geopotential height fields. It is not clear whether another choice of the norm would allow an accurate representation of both the three geopotential height fields and the two thicknesses with less than about 300 patterns.

c. EOFs of the atmosphere

From the 10 boreal winters of ECMWF analyses, we estimated the covariance matrix and computed the EOFs and their eigenvalues according to Eq. (2).

1) EIGENVALUES

(i) Spectrum of eigenvalues

The eigenvalue spectrum is steep. The first 83 EOFs account for 95% of the variance. It is a well-known fact that individual EOFs are not well resolved when neighboring eigenvalues are close together. To get an idea of the sampling error, we plotted the variances of the EOFs for each of the 10 winters in Fig. 3a. Averaging these 10 values would give the eigenvalue of the corresponding EOF. It turns out that even the dominant EOFs are not well resolved since the order of the EOFs changes from winter to winter (EOFs are ordered with respect to their variance). Much of the interannual variability projects onto these patterns, and many more years of observations would be required to accurately resolve the individual EOFs. For our purpose, it is not really necessary to resolve the individual EOFs accurately. We aim to partition the phase space into two subspaces, one that contains the flow structures that dominate the dynamics and another that contains the more or less slaved, low-energetic flow structures. For instance, the subspace spanned by the first 80 EOFs is well resolved from the subspace spanned by EOFs beyond index 100.

For the atmospheric EOFs, we also determined the error in the representation of atmospheric fields as a function of the EOF truncation. With 150 EOFs the mean representation error is about 13 m at 200 hPa, 10 m at 500 hPa, and 6 m at 800 hPa (see Fig. 4.)

(ii) Comparison between model and observations

In order to compare the model variability with observations, we computed the variances of the atmospheric EOFs in 10 independent 90-day periods in the 10 000-day time series of the T21 model. These variances are also plotted in Fig. 3a. Comparing the model and the observations, it turns out that the model has larger variability than the atmosphere. For EOFs with index beyond 400, the variance is more than 10 times larger. Reducing this aspect of the model drift might improve the forecast skill and climatology of the model.

It is worth noting that the pronounced difference in phase space structure between the model and the atmospheric attractor is not apparent from a comparison between the kinetic energy spectra. In Fig. 3b the kinetic energy spectrum is plotted for each of the 10 winters of ECMWF analyses for the Northern Hemisphere at 200 hPa for anomalies with respect to the winter mean. The same was done for 10 independent 90-day periods selected from the 10 000-day time series of T21. The model has less energy at total wavenumbers 1 and 2, more at wavenumbers 4 to about 10, and somewhat less at the very end of the spectrum. The picture is qualitatively the same at 500 and 800 hPa. Although the scale-selective diffusion is able to prevent the accumulation of energy at the tail of the spectrum and simulate about the right spectrum, it is not able to preserve the right phase relations between the spherical harmonics. Put differently, with the scale-selective diffusion, the model is not able to simulate the correct small-scale structures. Too much energy projects onto structures described by the trailing EOFs. A better closure might be to formulate the dissipation in terms of EOFs instead

of spherical harmonics. This will be investigated in section 6.

2) SPACE AND TIME CHARACTERISTICS

For the atmospheric EOFs, we also determined the autocorrelation of the amplitudes and the characteristic spatial scale. The results are plotted in Figs. 5a,b. As was the case for the model EOFs, the atmospheric EOFs are both a spatial as well as a time filter. Low (high) index EOFs predominantly project onto large(small)-scale waves and have a slow(fast) time dependence. Comparing the spatial-scale dependences (Figs. 2b and 5b), the main difference is that in case of the atmospheric EOFs the dominant spatial scale of EOFs between index 100 and 200 is smaller (approximately wavenumber 13) as compared to the model EOFs (wavenumber 11). Comparing the autocorrelations (Figs. 2a and 5a) it turns out that the atmosphere has a longer memory of the initial conditions.

4. EOF filtering and dissipation

Having determined the EOFs, they can be used in an attempt to improve the forecast skill and climate simulation of the model. Two methods are tested in section 6, which we will refer to as EOF filtering and EOF dissipation. In SE these methods were succesfully applied in a barotropic model. A brief outline of both is given in the section below.

a. EOF filtering

The model state is completely specified by the geopotential height at the three model pressure levels. In terms of EOFs, the state is given by a sum over the EOF patterns, multiplied by time-dependent amplitudes (usually referred to as principal components)

$$\Phi(\lambda, \phi, p, t) = \sum_{i=1}^{T} a_i(t) e_i(\lambda, \phi, p), \tag{4}$$

where λ and ϕ denote the geographical longitude and latitude, respectively, p is the pressure, and t is the time. The number of EOFs in the representation, T, can be varied. If in the representation T is smaller than the total number of EOFs, which is equal to the model's phase space dimension of 693, we say that the state is filtered on the first T EOFs.

Branstator et al. (1993) filtered ECWMF forecasts on the leading EOFs and found that the filtered forecasts verified better with filtered analyses than the unfiltered forecasts with unfiltered analyses. They concluded that the leading EOFs identify flow structures that are better predictable on average at longer lead times than the flow structures represented by the trailing EOFs. This is partly explained by the slower time evolution of the dominant EOFs (Fig. 5a). Another explanation might be that the model errors rapidly deteriorate the forecast for the trailing EOFs. In SE the trailing EOFs gained variance rapidly during the forecast due to the model error. Filtering on the dominant EOFs during the integration, not afterward as in Branstator et al. (1993), improved the forecasts for these EOFs.

The filter removes the contributions from the trailing EOFs to the tendency of the leading EOFs. This can easily be seen from the following expression for the tendency of the EOF amplitudes

$$\dot{a}_i(t) = \alpha_i + \sum_{j=1}^{N} \beta_{ij} a_j(t) + \sum_{j=1}^{N} \sum_{k=j}^{N} \gamma_{ijk} a_j(t) a_k(t), \quad \text{for } i = 1, \cdots, N, \tag{5}$$

where N is the dimension of the phase space of the model. Both the barotropic model as well as the baroclinic model of this paper lead to evolution equations of this form when formulated in terms of EOFs. The quadratic terms are due to the advection term in the model equations. If now the state is filtered on the leading $(N - 1)$ EOFs, which is equivalent to saying that a_N is put to zero, it is clear from Eq. (5) that the Nth EOF no longer contributes to the tendency of the leading $(N - 1)$ EOFs. If the state is filtered on the leading T EOFs at every time step during the model integration, it is the same as running an EOF model truncated to the leading T EOFs. Running an EOF model using Eq. (5) (usually referred to as the interaction coefficient method) is far more expensive than running the full T21 model with an EOF filter, except for severe truncations. The reason for this is that the T21 model makes use of the transform method, which is computationally attractive due to the efficient fast Fourier transform algorithm. An equivalent of the fast Fourier transform in case of an expansion into EOFs does not exist to our knowledge. In conclusion, an EOF model can be integrated at any truncation at about the cost of the full T21 model by integrating the T21 model with an EOF filter.

b. EOF dissipation

The filter introduced in the previous section can be looked upon as a kind of dissipation formulation. If energy is transferred to EOFs beyond truncation limit T, it is immediately dissipated. Another way to reduce the climate drift might be to dissipate energy at a finite timescale. The dissipation timescale can be tuned for each individual EOF as follows (see also SE). During a forecast, the variances of the EOF amplitudes start to diverge from the climatological variances due to the model error. We assume that the systematic effect of the neglected small-scale structures onto the resolved ones is mainly dissipative and that it can be adequately described by a linear dissipation term

$$\dot{a}_i(t) = \alpha_i + \sum_{j=1}^{T} \beta_{ij} a_j(t) + \sum_{j=1}^{T} \sum_{k=j}^{T} \gamma_{ijk} a_j(t) a_k(t) + \delta\beta_{ii} a_i(t), \quad \text{for } i = 1, \cdots, T, \tag{6}$$

that implies that the drift in the variance, determined from a set of forecasts, can be adequately described by

$$\text{var}(a_i(\tau)) = \text{var}(a_i(0)) e^{2\delta\beta_{ii}\tau} \quad \text{for } i = 1, \cdots, T, \tag{7}$$

where τ denotes the forecast day, and var(a_i) the variance of the ith EOF in the available set of forecasts.

The coefficients $\delta\beta_{ii}$ can be estimated from a set of forecasts by fitting Eq. (7) to the observed drift in variance or by solving Eq. (7) for $\delta\beta_{ii}$ at a particular time in the forecast τ,

$$\delta\beta_{ii}(\tau) = \frac{\ln\left(\frac{\text{var}(a_i(\tau))}{\text{var}(a_i(0))}\right)}{2\tau} \quad \text{for } i = 1, \cdots, T, \tag{8}$$

where ln() denotes the natural logarithm.

The EOF dissipation is introduced in the T21 model by projecting the model state at each time step onto the EOF basis, then calculating the dissipation and transforming back to physical space,

$$\dot{\Phi}(\lambda, \phi, p, t) = \sum_{i=1}^{T} \delta\beta_{ii} a_i(t) e_i(\lambda, \phi, p), \tag{9}$$

where $\dot{\Phi}$ denotes the contribution of the EOF dissipation to the geopotential height tendency.

5. First hypothesis

The first hypothesis is that EOFs capture the dynamics more efficiently than spherical harmonics. This hypothesis is tested in the two experiments described below.

a. The perfect model experiment

1) SETUP

To check the first hypothesis, the forecast skill of EOF truncated models is compared with the forecast skill of a T17 version. The skill is estimated from 200 10-day forecasts of the T21 circulation with a T17 version and EOF truncated models with varying numbers of EOFs.

The initial states were selected at 11-day intervals from the 2500-day dataset and subsequently first projected onto the first 150 EOFs and then truncated to T17. The choice of similar initial conditions makes a fair comparison of the forecast skill of the different models possible.

The EOF truncated runs were produced by using an EOF filter at every time step in T21 integrations. The total number of EOFs is 693, which equals the dimension of the T21 phase space. The truncations considered run from a minimum of 150 up to 500 EOFs in steps of 50 EOFs. A minimum of 150 EOFs is chosen because at this truncation the mean representation error of the geopotential height at 200, 500, and 800 hPa is comparable to or only slightly larger than present day analysis errors (see Fig. 1b). We considered all of these truncations since an objective criterion for truncation based on the spectrum of eigenvalues is not immediately obvious.

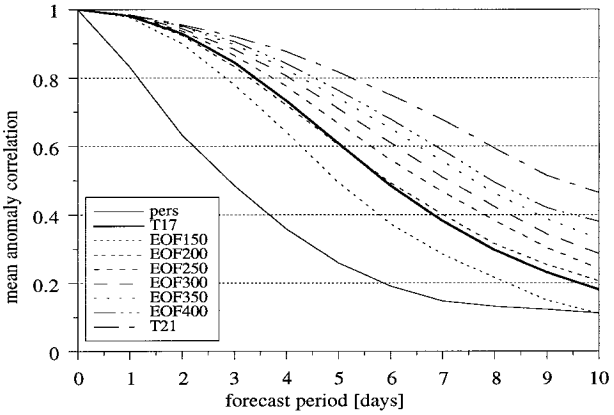

FIG. 6. Mean anomaly correlation coefficients of 200 10-day forecasts of the T21 circulation for persistence, T17, and EOF truncated models. The ACCs are calculated for 500-hPa geopotential height truncated to the first 150 EOFs.

2) RESULTS

The forecasts were verified by means of the rms error of the 500-hPa height and the anomaly correlation of 500-hPa height with respect to the mean state of the 10 000-day dataset. Prior to the verification, both the forecasted and the verifying fields were projected onto the first 150 EOFs.

Since the rms errors did not contain any additional information regarding the forecast skill, only the anomaly correlation coefficients (ACC) are shown and discussed. The mean ACCs of the 200 forecasts are plotted in Fig. 6 for persistence forecasts, T17, and the EOF models at various truncations. The persistence forecasts cross the 0.6 level around day 2, T17 at about day 5, and the perfect model at about day 8. The severest truncated EOF model, EOF150, crosses the 0.6 level at day 5. A monotonic increase in forecast skill is found as an increasing number of EOFs is retained in the model. With 200 EOFs, the EOF model has the same level of skill as T17, which has a 459-dimensional phase space. Evidently, a truncation in EOF space affects the dynamics less than a truncation in Fourier space. With 400 EOFs, the mean useful forecast range is still one day less than the perfect model. So the extremely low-variance EOFs still have a significant influence on the forecast skill.

This monotonic increase in forecast skill may not be so trivial as it seems. All models produce the same tendency initially since there is no interaction between

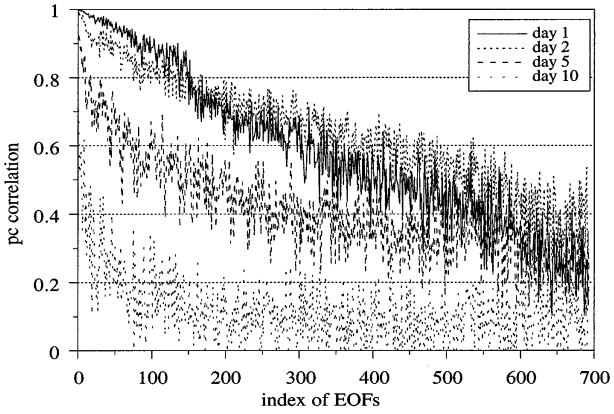

FIG. 7. Correlation between observed and predicted EOF amplitudes for 200 forecasts of the T21 circulation with T17 from initial conditions truncated to the first 150 EOFs. Negative values are not plotted.

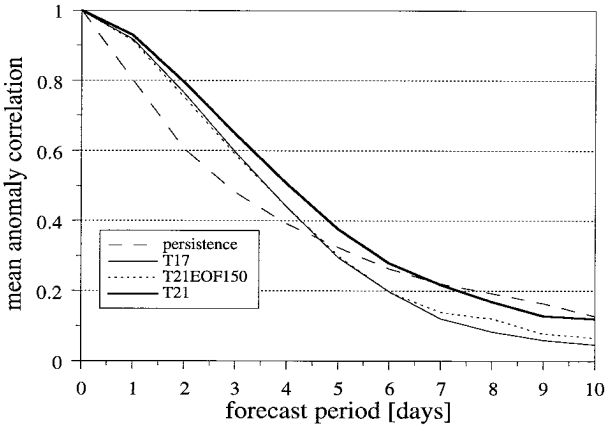

FIG. 8. Mean anomaly correlation coefficients of 80 10-day forecasts of the Northern Hemisphere in winter for persistence, T17, T21, and T21 filtered on the leading 150 EOFs.

the first 150 EOFs and the remaining ones initially due to the special choice of the initial condition. However, in due course of the integration, EOFs beyond index 150 become excited and start interacting with the leading EOFs. The effect of this feedback on the evolution of the leading EOFs becomes appreciable within a couple of days and improves the forecast skill significantly. This result indicates that an increased resolution improves the forecast skill of the dominant flow structures, even when the resolved small scales are not properly initialized. The forecast skill of the perfect model (T21) for the individual EOFs is analyzed by calculating the correlation between the time series of the forecasted and observed amplitude. Figure 7 shows this correlation at day 1, 2, 5, and 10 of the forecast. The first thing to note is that the forecast skill is a function of EOF index: the dominant EOFs are better forecasted. This result is in agreement with the results obtained by Branstator et al. (1993), who did a similar analysis for ECMWF forecasts. Second, although EOFs beyond index 150 have zero initial amplitude, there is skill in forecasting these modes at day 1 and even more so at day 2. It seems that to a certain extent the trailing EOFs are slaved to the leading EOFs, adjusting quite rapidly to the state of the leading EOFs.

b. The ''real world'' experiment

Starting from 1 December, we made eight nonoverlapping forecasts of 10 days for each of the 10 winters with the T21 model, a T17 version, and an EOF truncated version with 150 EOFs. All forecasts are started from initial conditions that are first truncated to the leading 150 EOFs and next to T17 to make a fair comparison of the forecast skill of the different models possible.

Figure 8 contains the mean ACCs of the 80 forecasts. The forecasts are verified after projecting forecasts and analyses onto the first 150 EOFs. It was verified that the projection hardly affected the mean ACCs. The mean useful forecast range of the T21 model turns out to be approximately 3.5 days, a gain of 1.5 days over persistence. For comparison, the current useful forecast range of the ECMWF model for the 500-hPa geopotential height field of the Northern Hemisphere extratropics in winter is about 6.5 days. With 150 EOFs, the EOF model has the same level of skill as T17, which has a 459-dimensional phase space. Also in this experiment in which the model error is large and not only due to a limited horizontal resolution, it turns out that EOFs describe the dynamics more efficiently than spherical harmonics.

To conclude this section, we can state that a basis of EOFs more efficiently captures the dynamics than a basis of spherical harmonics in terms of the number of phase space coordinates needed. However, EOFs with variances four orders of magnitude smaller than the leading EOF still contribute significantly to the forecast skill of the leading EOFs. The trailing EOFs are to some extent slaved to the leading ones, which gives some hope that a parameterization of their influence on the evolution of the leading EOFs is possible.

6. The second hypothesis

In this section the hypothesis is tested that the forecast skill and climatology of the model can be improved by using EOFs as basis functions. The methodology was explained in section 4. The hypothesis is first tested in the perfect model experiment, then in the ''real world'' experiment.

a. The perfect model experiment

In practice, EOFs are estimated with limited resolution only. The resolution is at most the resolution of the model. Therefore, in the context of this idealized experiment, EOFs will be used that are calculated at T17

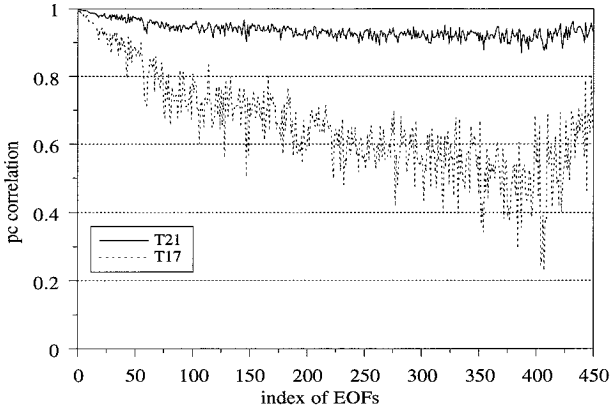

FIG. 9. Correlation at day 2 between observed and predicted EOF amplitudes as determined from 200 forecasts of the T21 circulation with T17 and T21 from initial conditions truncated to T17.

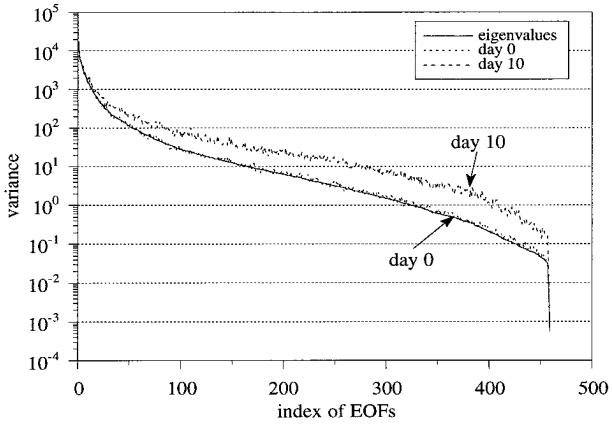

FIG. 10. Drift of T17 measured by the variances of the EOFs, calculated at day 0 and day 10 of 200 T17 forecasts. For comparison, the variances of the EOFs in the 10 000-day time series is plotted.

resolution in an attempt to improve the forecast skill of T17 by reducing the effect of the model error.

1) IMPACT OF MODEL ERROR

To investigate the effect of the model error on the forecast skill of the EOFs, we repeated the forecast experiment of section 5a but this time starting from T17 truncated initial conditions with both the perfect model (T21) and T17. The error in the T21 forecasts is solely due to the error in the initial condition. The correlation at day 2 between predicted and observed EOF amplitude is plotted in Fig. 9 for the T17 and T21 forecasts. Comparing both graphs, it is evident that the model error dominates the internal error growth and rapidly degrades the forecasts for the trailing EOFs in the T17 forecasts. One reason for the rapid loss of skill is that the trailing EOFs gain variance. Figure 10 shows the variance of the EOFs in the 200 forecasts with T17 at day 0 and at day 10. Note first that the sampling error is small. Although we have a sample of only 200 days, separated by intervals of 11 days, the variance at day 0 is close to the variance calculated from the 10 000-day dataset (curve labeled eigenvalues). At day 10 however, the variance of the trailing EOFs has increased significantly. We hypothesize that either filtering the trailing EOFs during the T17 forecasts or increasing the dissipation on these EOFs will improve the forecast skill of the leading EOFs.

2) EOF FILTER

We repeated the forecast experiment with T17, this time filtered every time step on a fixed number of EOFs. The mean anomaly correlation coefficients are plotted in Fig. 11. All forecasts started from the same initial conditions, which were truncated to the first 150 EOFs. The forecasts are verified on the first 150 EOFs. A monotonic increase of forecast skill is found as the number of EOFs retained in the filter is increased. With 350 EOFs or more, the forecast skill is as good as the full T17 model, which has 459 degrees of freedom. However, we do not find an improvement of forecast skill by filtering every time step on a limited number of EOFs. This is to be contrasted with the results of SE in the barotropic case. There it was shown that the forecast skill of a T20 version of a barotropic T21 model improved substantially by filtering the model state after each day of integration on the first 20 EOFs. Unpublished results revealed that the skill also improved by filtering every time step on the first 20 EOFs.

3) EOF DISSIPATION

(i) Influence on forecast skill

The EOF filter did not improve the forecast skill. We may try to reduce the drift of T17 and improve its prediction skill by an additional dissipation on the trailing

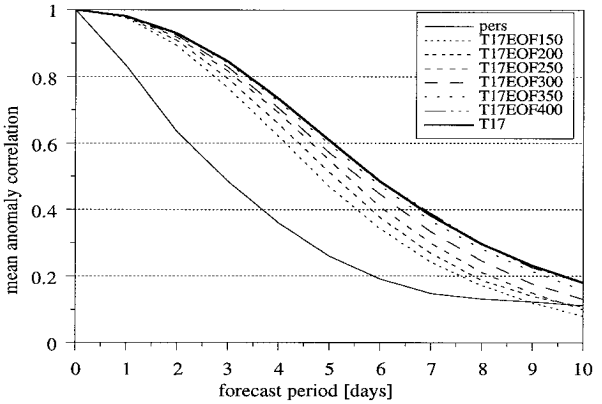

FIG. 11. Mean anomaly correlation coefficients of 200 10-day forecasts of the T21 circulation for persistence, T17, and EOF truncated models. The ACCs are calculated for 500-hPa geopotential height truncated to the first 150 EOFs.

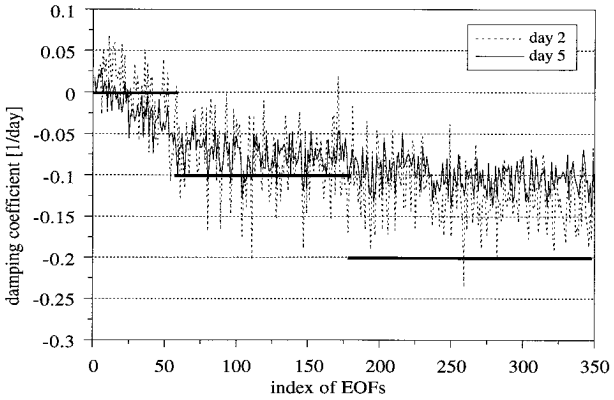

FIG. 12. Empirical damping coefficients estimated from 200 T17 forecasts of the T21 circulation at forecast day 2 and day 5. Assuming an exponential growth of the variance of the EOFs, these damping coefficients balance the drift. The values according to the thick solid line are used in subsequent experiments.

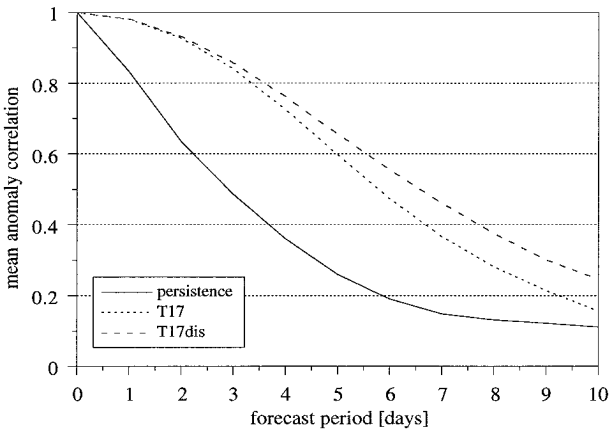

FIG. 13. As in Fig. 8 but for persistence forecasts, T17, and T17 with empirical dissipation according to Fig. 12 (T17dis).

EOFs in order to prevent an accumulation of variance on these EOFs. We assume that the systematic effect of the neglected small-scale structures onto the resolved ones is mainly dissipative and that it can be adequately described by a linear dissipation term (see section 4). The drift in variance of the first 350 EOFs is estimated from the 200 10-day forecasts with T17 starting from T17 initial conditions. The analysis is limited to the first 350 EOFs since T17 filtered on the leading 350 EOFs has the same forecast skill as the full T17 model. Apparently, the trailing EOFs beyond 350 do not contribute significantly to the dynamics and will be filtered in the sequel. The coefficients $\delta\beta_{ii}$ are estimated from Eq. (8). A plot of these estimates is shown in Fig. 12 for forecast days 2 and 5. For most EOFs, the two estimates are not too far off, which indicates that the variance increases approximately exponentially during this period. The strength of the dissipation increases with increasing EOF index, which implies that the dissipation is scale selective. The small scales are damped more efficiently. The damping timescale is of the order of days, so we may expect an effect on the forecast skill. Guided by these two curves, damping coefficients were chosen as given by the thick solid line. That we chose a somewhat stronger dissipation on the trailing EOFs as indicated by the drift deserves some explanation. At first, we applied the damping coefficients as estimated from the drift at day 2. It turned out that the EOFs at the tail still drifted, gaining too much variance. Apparently, a stronger dissipation was required to prevent this drift.

With the additional dissipation as indicated by the thick solid line in Fig. 12, the T17 forecasts were repeated. The mean ACCs are plotted in Fig. 13 (curve labeled T17dis). Compared to forecasts without a correction for the drift, the mean useful forecast range increases with about half a day.

(ii) Influence on climate simulation

The impact on the forecast skill of the empirical dissipation on the EOFs is small. The additional dissipation might be more relevant with respect to the climatology of the model. Therefore a 2500-day integration with T17 was performed to establish its climatology. T17 with the EOF dissipation as given by the thick solid line in Fig. 12, was also integrated for 2500 days to check whether its climatology is closer to the truth (T21) compared to T17. Of both runs, the first 500 days were discarded. In Fig. 14 the variance of the EOFs in the two runs is plotted and compared with the variance of the EOFs in the 10 000-day T21 run. The variance of the trailing EOFs is overestimated in T17 but well simulated in T17dis. However, the variance of the leading EOFs, especially of the first one, is underestimated in T17dis.

For both runs, we calculated the variance of 500-hPa geopotential height for 10-day running means and daily deviations from 10-day running means. The results (not

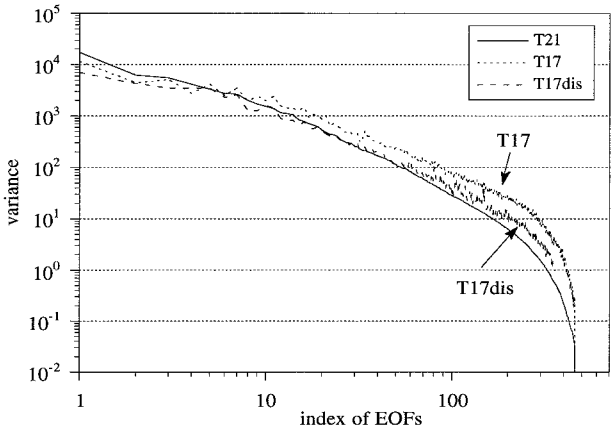

FIG. 14. Variance of EOFs in the 10 000-day time series of T21, in a 2000-day time series of T17, and in a 2000-day time series of T17 with empirical dissipation to balance the initial drift (T17dis).

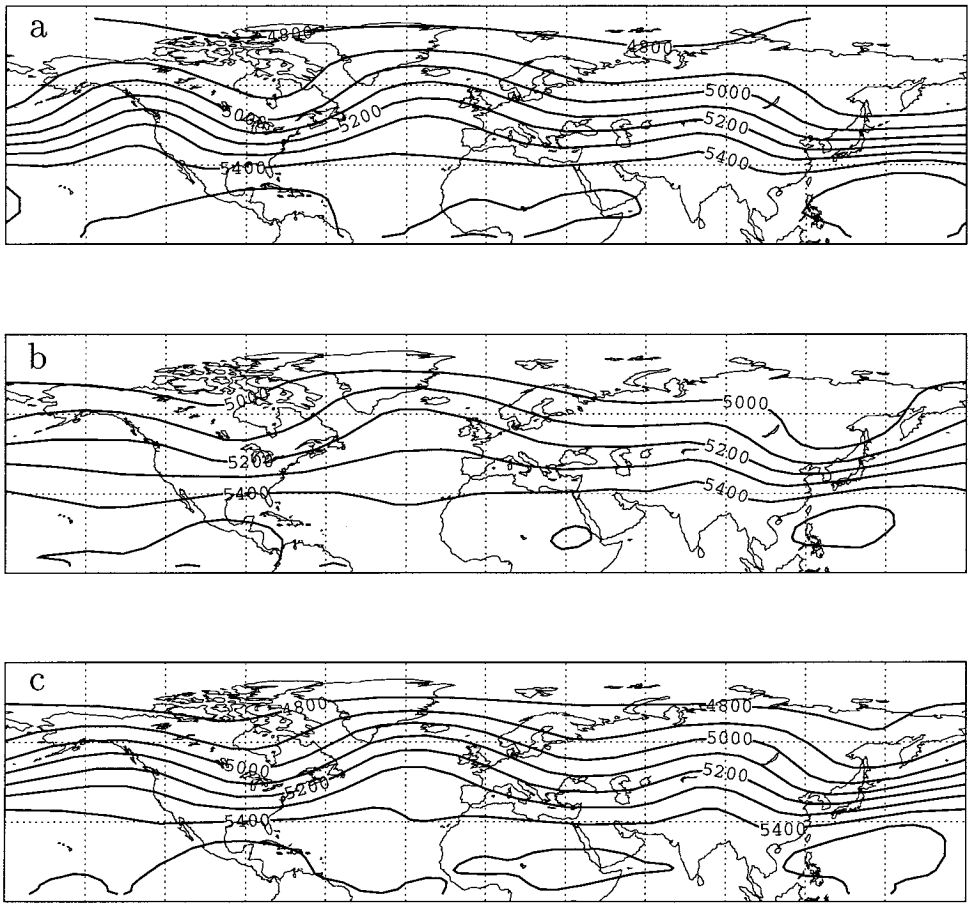

FIG. 15. Mean 500-hPa geopotential height of (a) the 10 000-day time series of T21, (b) a 2000-day time series of T17, and (c) a 2000-day time series of T17 with empirical dissipation to balance the initial drift (T17dis).

plotted) show that the low-frequency variance, which is dominated by the first EOF, is underestimated in T17 and even more so in T17dis. The high-frequency variance, overestimated in T17, is better simulated in T17dis. Although the model has been corrected to reduce the drift of the variance, it turns out that the mean state has improved as well. In Fig. 15, the mean 500-hPa geopotential height is plotted for T21, T17, and T17dis. Compared to T21, the strength of the mean circulation is greatly reduced in T17. In T17dis the mean circulation is much better simulated.

To summarize, the EOF filter did not improve the forecast skill, in contrast to previously obtained results in the barotropic case (SE). The empirical EOF dissipation gave a small improvement of the forecast skill, but had a larger impact on the climate simulation. The mean and high-frequency variability were improved, the low-frequency variability remained too low.

b. The ''real world'' experiment

In this section an attempt is made to improve the skill of T21 in predicting the evolution of the Northern Hemisphere winter circulation and its ability to simulate the winter climatology. For this purpose, EOFs of the ECMWF analyses are used (see section 3).

1) IMPACT OF MODEL ERROR

The climate drift of T21 is diagnosed from the set of 80 forecasts of section 5b by computing the variance of the atmospheric EOFs at each day in the forecast. In Fig. 16, the variance is plotted for day 0, 1, and 10. Within 1 day, the variance of the trailing 500 EOFs increases significantly. Within 10 days, the trailing EOFs have reached their (model) climatological values. In an attempt to reduce this aspect of the climate drift, first the EOF filter is applied to T21, second EOF dissipation is introduced.

2) EOF FILTER

In a first attempt to improve the forecast skill, forecasts were produced with an EOF filter applied every time step to the model state. The number of EOFs retained in the filter ran from 150 up to 500 EOFs with

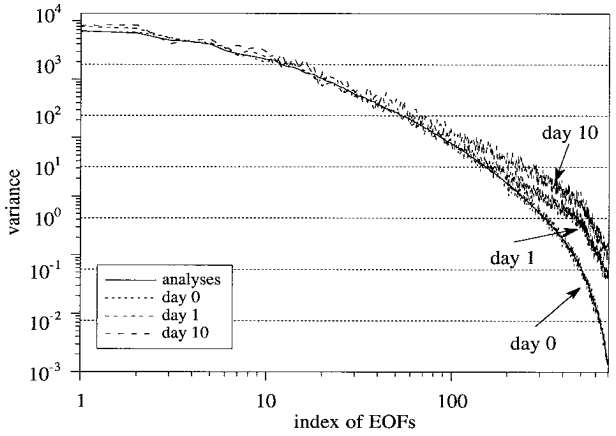

FIG. 16. Drift of T21 measured by the variances of the EOFs, calculated at day 0, day 1, and day 10 of 80 T21 forecasts. For comparison, the variances of the EOFs in the 10 winters of ECMWF analyses are plotted.

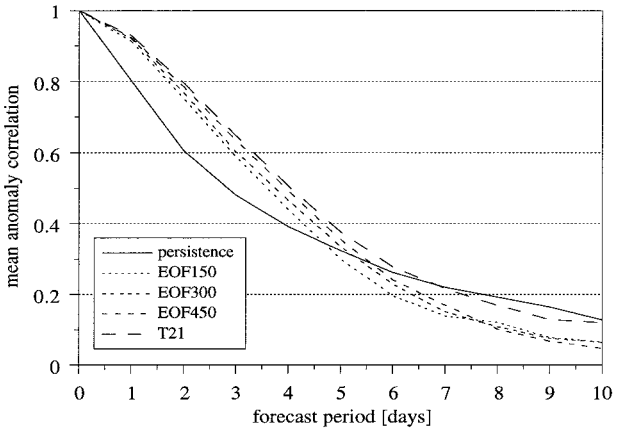

FIG. 17. Mean anomaly correlation coefficients of 80 10-day forecasts of the Northern Hemisphere in winter for persistence, T21, and T21 filtered on an increasing number of EOFs.

steps of 50 EOFs. All EOF truncated runs started from initial conditions truncated to the first 150 EOFs to make a fair comparison possible. The mean ACCs of T21 and the EOF truncated models for truncation limits 150, 300, and 450 EOFs are plotted in Fig. 17. In the range of useful forecasts, a monotonic improvement is noted as an increasing number of EOFs is retained in the model. The EOF filter degrades the forecast skill throughout the whole forecast range. With 150 EOFs out of a total of 693, the average useful forecast range reduces to about 3 days. In contrast to the results of SE in the barotropic case, the EOF filter does not improve the forecast skill of the unfiltered model.

3) EOF DISSIPATION

(i) Influence on forecast skill

In a second attempt to improve the forecast skill, a linear dissipation on the EOFs is introduced as in the perfect model experiment [Eq. (8)]. Since all EOFs contribute to a better predictive skill, all EOFs are retained. The estimated strength of the dissipation for each of the EOFs is plotted in Fig. 18 for forecast day 1, 2, and 3. Again, the estimated dissipation turns out to be strongly scale selective. The three estimates for EOFs beyond index 300 differ substantially, which implies that the variance does not increase exponentially. Note that the drift in the ''real world'' experiment is much more rapid compared to the perfect model experiment. For the trailing EOFs an *e*-folding timescale less than 1 day is found whereas in the perfect model experiment the drift of T17 has an *e*-folding timescale of 5–10 days. In the latter case, a limited horizontal resolution is the only error source. In the former case, other important error sources are, for instance, the coarse vertical resolution, the representation of diabatic sources and sinks by the empirically determined constant potential vorticity forcing, the representation of the orographic forcing, and the quasigeostrophic approximation.

The dissipation was approximated by the solid thick line in Fig. 18. With these dissipation coefficients, the forecast experiment was repeated. The mean ACCs (not plotted) were hardly affected by the empirically determined dissipation. In contrast to the perfect model experiment, it turns out that reducing this aspect of the model drift has no significant effect on the forecast skill. Probably, in this case the contribution of the trailing EOFs to the forecast error evolution of the leading EOFs is small compared to the other model error sources mentioned. These model error sources can not be adequately described by a linear dissipation on the EOFs.

(ii) Influence on climate simulation

Although the empirical correction has no effect on the forecast skill, it might improve the climatology of

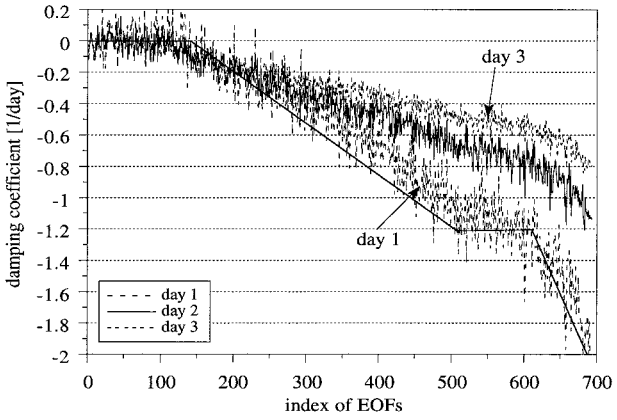

FIG. 18. Empirical damping coefficients estimated from 80 T21 forecasts of the Northern Hemisphere in winter at forecast day 1, day 2, and day 3. Assuming an exponential growth of the variance of the EOFs these damping coefficients balance the initial drift. The values according to the thick solid line are used in subsequent experiments.

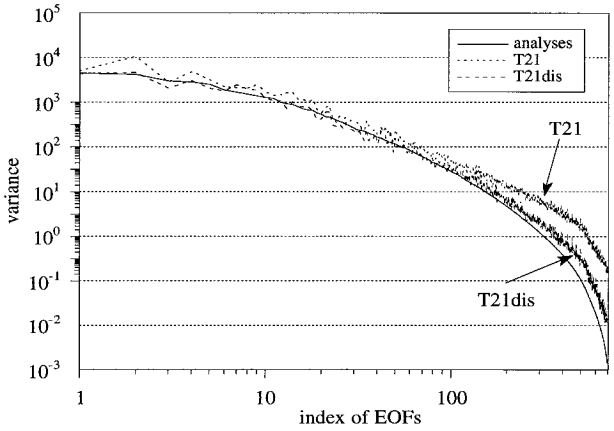

FIG. 19. Variance of EOFs in the 10 winters of ECMWF analyses, in a 10 000-day time series of T21 and in a 2000-day time series of T21 with empirical dissipation to balance the initial drift according to Fig. 18 (T21dis).

the model. Therefore, with and without the dissipation coefficients plotted in Fig. 18, the model was integrated for 2500 days. The first 500 days were discarded. From the remaining 2000 days, the variances of the EOF amplitudes and the mean 500-hPa geopotential height and its daily variability were calculated. The variances of the EOF amplitudes are plotted in Fig. 19 for T21, T21dis, and the 10 winters of ECMWF analyses. The variances of T21dis are closer to the observed variances. Despite the strong dissipation, the variances of the trailing EOFs, although small, are still too large. The spatial pattern of daily 500-hPa geopotential height variability is plotted in Fig. 20. The variability has been reduced in T21dis, especially in the polar areas and the spatial pattern is closer to the observations. The mean 500-hPa height field is plotted in Fig. 21. The jet maximum over the Atlantic is better simulated in T21dis, but in other areas the circulation is too strong and is better simulated in T21.

To conclude we can say that trying to improve the forecast skill of T21 by merely truncating the trailing EOFs or by an empirically determined dissipation on the EOFs was not succesful. The empirically determined

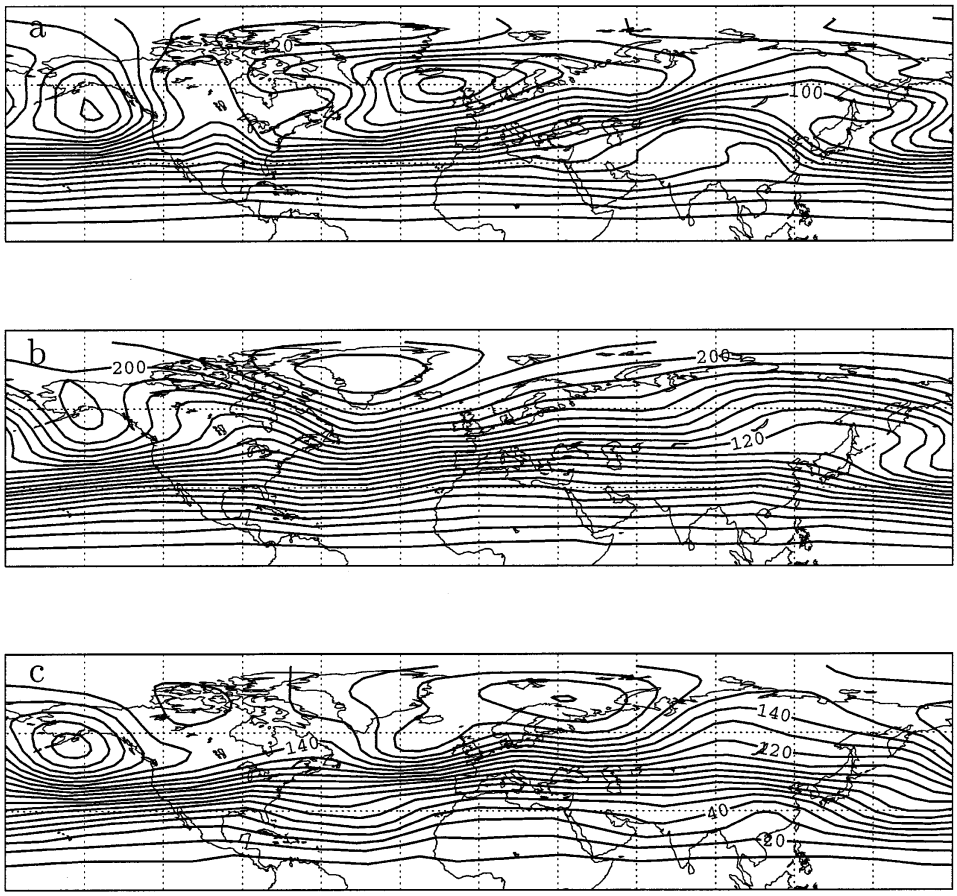

FIG. 20. Daily variability of 500-hPa geopotential height of (a) the 10 winters of ECMWF analyses, (b) the 10 000-day time series of T21, and (c) a 2000-day time series of T21 with empirical dissipation to balance the initial drift according to Fig. 18 (T21dis).

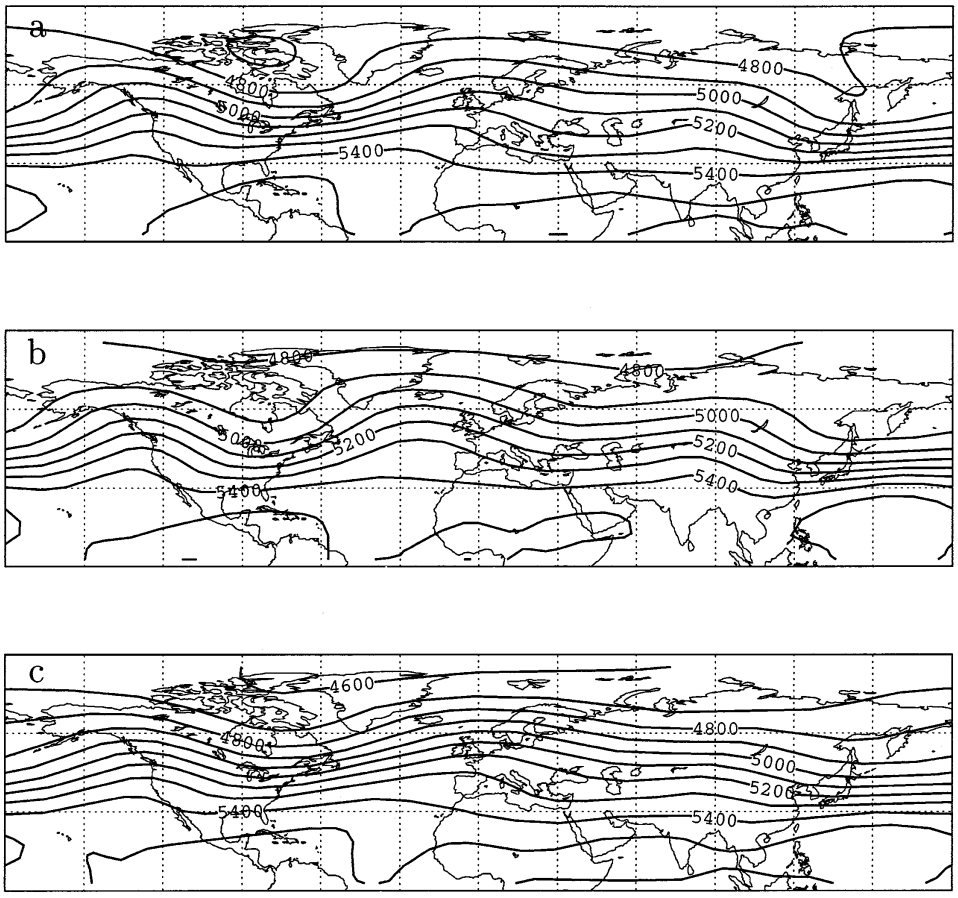

FIG. 21. Mean 500-hPa a height field of (a) the 10 winters of ECMWF analyses, (b) the 10 000-day time series of T21, and (c) a 2000-day time series of T21 with empirical dissipation to balance the initial drift according to Fig. 18 (T21dis).

dissipation on the EOFs resulted in some improvement of the simulated atmospheric variability.

7. Discussion and conclusions

In this study, we investigated the merits of using EOFs as basis functions in a baroclinic model of the atmosphere. A quasigeostrophic, hemispheric, three-level T21 model (693-dimensional phase space) was used in two experiments. In the first experiment, a perfect model approach was taken. Model errors were introduced by reducing the horizontal resolution, EOFs were derived from a long model integration. In the second experiment, T21 was used to produce forecasts for the Northern Hemisphere in winter. EOFs were derived from ECWMF analyses.

Two hypotheses were tested. The first hypothesis is that a basis of EOFs is more efficient in describing large-scale atmospheric dynamics compared to spherical harmonics. The second hypothesis is that the forecast skill and climatology of the model can be improved by using EOFs as basis functions.

The first hypothesis was tested in both experiments by comparing the predictive skill of EOF truncated models and a T17 version of the T21 model. It was found that with less than half the number of phase space dimensions the EOF truncated model had the same predictive skill as T17. However, the EOF truncated model is computationally more expensive since an equivalent of the fast Fourier transform for EOFs does not exist.

One could live with the fact that using EOFs as basis functions is more expensive if the second hypothesis of this paper were true: predictions and/or climate simulations with EOF-based models are superior to traditional spectral models. In Selten (1995a) encouraging results were obtained in a barotropic model using an EOF filter and a dissipation formulation in terms of EOFs. However, in the baroclinic model of this study, an EOF filter did not result in better predictions. In the perfect model experiment, the forecast skill and the climate simulation of T17 were somewhat improved by the introduction of the EOF dissipation. However, in the second experiment, the EOF dissipation did not significantly improve the ability of T21 to simulate the Northern Hemisphere winter circulation. In the former case, a reduced horizontal resolution is the only error source.

In the latter case, other important error sources are, for instance, the coarse vertical resolution, the representation of diabatic sources and sinks by the empirically determined constant potential vorticity forcing, the representation of the orographic forcing, and the quasigeostrophic approximation. Apparently, the systematic effect of these model errors cannot be adequately described by a linear dissipation on the EOFs.

The present results in the baroclinic case are not very encouraging. Nevertheless, the present study may be regarded as just a first attempt and the method might be improved upon. Probably the present choice of empirical basis functions is not optimal and no doubt the empirical linear dissipation on the EOFs as a parameterization for the model error can be improved upon. Arguments and suggestions are given below.

Probably the variance criterion used in the definition of the EOFs is not optimal. For instance, it was verified that T17, on average, better represents an arbitrary state on the T21 attractor than a representation with 200 EOFs. However, the dynamics is better described by the 200 EOFs. This implies that optimizing a representation with respect to the variance will not necessarily yield a representation that is optimal in describing the dynamics. Thus there might be a set of basis functions that at a given truncation better describes the dynamics compared to EOFs, although the amount of variance explained by these functions is less. This is likely to be the case. In the perfect model experiment it was found that with 400 EOFs the mean useful forecast range is still one day less than the perfect model (693 EOFs). So the extremely low-variance EOFs still have a significant influence on the forecast skill. This problem is connected to the problem of choosing a norm in phase space to measure distances between phase points. The norm that we have chosen in the definition of the variance and the EOFs is probably not the optimal one. The choice of a suitable norm certainly deserves more investigation.

An alternative way to determine basis functions that better capture the dynamics is given by Hasselmann (1988). He described a general method to derive a set of basis functions [referred to as principal interaction patterns (PIPs)] that minimizes the tendency error in a least squares sense. Kwasniok (1996) applied this technique to the barotropic model of SE and found a set of PIPs that better captures the dynamics compared to EOFs, although the amount of variance explained by the PIPs is less. A drawback of the PIP approach is that the method becomes prohibitively expensive in high-dimensional phase spaces (order 100).

To be able to still make use of the fast Fourier transform and at the same time reduce the number of expansion functions, one could limit the EOF or PIP expansion to the meridional direction and replace the associated Legendre functions in the spherical harmonics by an orthogonal set of EOFs or PIPs. This might lead to a description that is more efficient than traditional models in terms of computational resources. The idea is to use EOFs of the form $G_{mnl}(p)E_{mn}(\phi)\exp(im\lambda)$ instead of $E(p, \phi, \lambda)$ as in the present study. This approach for the horizontal representation might lead to a more efficient description, since in the meridional direction, the atmospheric variability is very inhomogeneous with most variability at latitudes where the jet meanders. Thus probably the number of meridional basis functions can be significantly reduced by using meridional EOFs of the form $E_{mn}(\phi)$, especially for low zonal wavenumbers m for which in a triangular truncation T there are the most Legendre functions retained ($T - m$). However, since the computational cost is only linear in the number of meridional basis functions used, the computational gain will probably be limited.

With respect to the representation of the vertical structure in terms of EOFs, it is hard to say anything about the performance of such a model. To our knowledge, the first attempts to formulate a model using a three-dimensional spectral representation were not very successful (Machenhauer and Daley 1974). If a realistic spectral model in three dimensions could be formulated using theoretical basis functions, then it would be worthwile to try EOFs for the vertical structure since Holmström (1963), for instance, has shown that the large-scale vertical structure of the atmosphere is well described by only a few EOFs.

The results in this paper suggest that the empirically determined dissipation as a parameterization of the systematic effect of the model error is only marginally successful. Other parameterizations might be formulated that perform better: for instance, a combination of the current parameterization, the approach of Sausen and Ponater (1990), and the statistical closure developed in Selten (1997) along the lines of a proposition made by Leith (1978). In any case, to substantially improve the forecast skill, the nonsystematic part of the model error needs to be more accurately parameterized.

Acknowledgments. I am indebted to Dr. Theo Opsteegh for his support and advice during this research and his comments on the first draft of this paper. Dr. Franco Molteni is kindly acknowledged for allowing me to use the code of his model.

REFERENCES

Boer, G. J., 1984: A spectral analysis of predictability and error in an operational forecast system. *Mon. Wea. Rev.,* **112,** 1183–1197.

Branstator, G., A. Mai, and D. Baumhefner, 1993: Identification of highly predictable flow elements for spatial filtering of medium- and extended-range forecasts. *Mon. Wea. Rev.,* **121,** 1786–1802.

Hasselmann, K., 1988: PIPs and POPs: The reduction of complex dynamical systems using principal interaction and oscillation patterns. *J. Geophys. Res.,* **93,** 11 015–11 021.

Holmström, I., 1963: On a method for parametric representation of the state of the atmosphere. *Tellus,* **15,** 127–149.

Kwasniok, F., 1996: The reduction of complex dynamical systems using principal interaction patterns. *Physica D,* **92,** 28–60.

Leith, C. E., 1978: Objective methods for weather prediction. *Annu. Rev. Fluid Mech.,* **10,** 107–128.

Liu, Q., and J. D. Opsteegh, 1995: Interannual and decadal variations of blocking in a quasi-geostrophic model. *Tellus,* **47A,** 941–954.

Lorenz, E. N., 1963: Deterministic, nonperiodic flow. *J. Atmos. Sci.,* **20,** 130–141.

——, 1982: Predictability experiments with a large numerical model. *Tellus,* **36A,** 98–110.

Machenhauer, B., and R. Daley, 1974: A baroclinic primitive equation model with a spectral representation in three dimensions. Institute of Theoretical Meteorology, University of Copenhagen Rep. No. 4, 62 pp. [Available from Institut for Teoretisk Meteorologi, Haraldsgade 6, DK 2200 Copenhagen, Denmark.]

Marshall, J., and F. Molteni, 1993: Toward a dynamical understanding of planetary-scale flow regimes. *J. Atmos. Sci.,* **50,** 1792–1818.

Rinne, J., and V. Karhila, 1975: A spectral barotropic model in horizontal empirical orthogonal functions. *Quart. J. Roy. Meteor. Soc.,* **101,** 365–382.

Sausen, R., and M. Ponater, 1990: Reducing the initial drift of a GCM. *Beitr. Phys. Atmos.,* **63,** 15–24.

Schubert, S. D., 1985: A statistical-dynamical study of empirically determined modes of atmospheric variability. *J. Atmos. Sci.,* **42,** 3–17.

Selten, F. M., 1993: Toward an optimal description of atmospheric flow. *J. Atmos. Sci.,* **50,** 861–877.

——, 1995a: An efficient description of the dynamics of barotropic flow. *J. Atmos. Sci.,* **52,** 915–936.

——, 1995b: An efficient description of large-scale atmospheric dynamics. Ph.D. thesis, Free University Amsterdam, 169 pp. [Available from KNMI, P.O. Box 201, 3730 AE De Bilt, the Netherlands.]

——, 1997: A statistical closure of a low-order barotropic model. *J. Atmos. Sci.,* **54,** 1085–1093.